Extreme Mechanics Letters 35 (2020) 100643

Contents lists available at ScienceDirect

Extreme Mechanics Letters

journal homepage: www.elsevier.com/locate/eml

Mechanics-guided design of shape-morphing composite sheets with hard and soft materials

Burebi Yiming, Tao Liu, Guodong Nian, Zilong Han, Zheng Jia *, Shaoxing Qu

Key Laboratory of Soft Machines and Smart Devices of Zhejiang Province, Center for X-Mechanics, Department of Engineering Mechanics, Zhejiang University, Hangzhou, 310027, China

ARTICLE INFO

Article history:
Received 10 December 2019
Received in revised form 22 January 2020
Accepted 28 January 2020
Available online 30 January 2020

Keywords:
Finite element modeling
Composite hydrogels
Folding axis
Shape transformation

ABSTRACT

Nature abounds with structures capable of changing shapes upon exposure to stimuli. These shape-morphing structures (for instance, the conifer pinecone) are often comprised of passive hard phases embedded in active soft materials that are stimuli-responsive. Although enthusiasm in mimicking the shape-changing phenomena in natural systems has induced an impetus to develop various artificial self-shaping structures, the effect of hard phases on the shape transformation and its underlying mechanics have not been systematically investigated. In this paper, we conduct finite element modeling to simulate the shape transformation of hybrid composite sheets consisting of fibers embedded in the hydrogel matrix, which is a widely employed approach to construct self-folding structures. It is revealed that the orientation of the folding axis is dictated by the hard fibers when the fiber modulus is sufficiently larger than that of the hydrogel matrix. Guided by the mechanics analysis, we construct self-folding composite sheets by incorporating 3D-printed stiff polylactic acid (PLA) patterns into soft poly(*N*-isopropylacrylamide) (PNIPAm) gels. The modulus of PLA exceeds that of PNIPAm by five orders of magnitude. Upon stimulation of elevated temperature, the PNIPAm/PLA composite sheets exhibit directional folding with folding axis parallel to the hard PLA strips, contrasting with most reported hybrid hydrogel sheets in which folding axes were perpendicular to the embedded fibers. Various 3D morphologies, including tubes, helices, scrolls, have been achieved by programming the embedded PLA patterns. We also generate an analog of curled leaves and the results offer mechanistic understandings of the curling process of leaves in nature. We hope this work can provide guidance for designing self-shaping soft machines that are made by integrating hard and soft materials together.

1. Introduction

Shape-transformation phenomena of plants are ubiquitous in nature. For example, Venus flytrap snaps shut rapidly via snap-through instability due to the cell-regulated turgor release [1]. The shape change of lily during blossom is attributed to the faster growth of the petal margins relative to the center [2]. These shape-changing phenomena are enabled by active cellular activities of living tissues such as metabolism and cell proliferation. In addition, many non-living plant tissues change shape via a passive hydro-responsive mechanism. Ice plants disperse their seeds by passively unfolding protective layers on the seed capsules when sufficiently hydrated by water [3]. Likewise, wheat awns [4], and pods [5] release their seeds by hydration/dehydration-induced deformation upon changes in air humidity. These plant tissues and organs are dead and, compared with self-shaping driven by complex cellular activity, their metabolism-independent hydro-responsive mechanisms are more amenable to transfer into designs of man-made materials capable of programmable self-shaping capabilities.

The enthusiasm in mimicking the phenomena of shape transformation that nature has perfected over billions of years has induced an impetus to develop a new class of man-made structures: stimuli-responsive and shape-morphing structures. These structures, which usually transform from 2D planar shape into 3D configurations when subjected to external stimuli, have enabled a broad range of applications including reconfigurable devices [6,7], self-folding robots [8], drug delivery containers [9], and actuators [10]. Among all materials that change volume on command, hydrogels are emerging as a prime candidate for constructing stimuli-responsive and self-morphing structures because of the high water content which provides physical similarity to living tissues and the responsiveness to multiple stimuli including temperature [11,12], pH [13], ionic strength [14,15], light [16,17], enzyme [18], magnetic field [19,20], etc. One should recognize that plant tissues and organs feature heterogeneous structures that consist of different regions of distinct material properties. The shape change of plants occurs from the deformation mismatch between different regions of tissues. Thereby, the most

* Corresponding author.
E-mail address: zheng.jia@zju.edu.cn (Z. Jia).

https://doi.org/10.1016/j.eml.2020.100643
2352-4316/

common strategy to develop man-made programmable and responsive structures is to combine hydrogels of different kinds in a single composite. Hydrogel sheets with in-plane heterogeneous structures have been adopted to engender complex 3D structures via buckling induced by mechanical mismatch [14,21–25]. Driving force for shape changing of hydrogels with in-plane heterogeneities is often limited, resulting in either small amplitude of shape-transformation or long response time. As a result, hybrid hydrogel sheets with both in-plane and out-of-plane heterogeneous properties have been fabricated to create complex 3D shapes upon external stimuli [12,15,18,26–31], with the out-of-plane gradients offering additional deformation driving force via bending. The abovementioned hybrid samples mainly consist of soft constituent materials. In stark contrast, biological materials in nature program their structures by using both hard and soft materials. For instance, the pinecone scale is comprised of a soft tissue matrix reinforced by stiff cellulose fibers. The anisotropic deformation of the soft matrix restricted by the stiff fibers gives rise to macroscopic changes in shape [32]. Several synthetic stimuli-responsive architectures made by integrating hard and soft materials have been reported [33–36]. For example, trilayer structures consisting of rigid plastic strips sandwiching a swellable temperature-responsive hydrogel are reported and the formation of concatenated multiple helices is demonstrated [33]. Nevertheless, in these studies, the fundamental mechanics underpinning how hard strips/fibers determine the important features of shape transformation (e.g. the folding axis) has not been systematically investigated.

Herein, by resorting to the finite element method (FEM), we model the shape transformation of hybrid composite sheets consisting of reinforcement strips embedded in the hydrogel matrix, a widely utilized approach to fabricate self-folding structures. It is demonstrated that the folding axis of the rolled state of the composite sheets orients parallel to the hard strips when the strip modulus is significantly larger than that of the hydrogel matrix. Enabled by mechanistic understanding from mechanics analysis and recent advances in exploiting additive manufacturing to create shape-changing structures [37–39], we report a novel 2D self-shaping composite sheets by incorporating 3D-printed stiff polylactic acid (PLA) fibers into soft poly(*N*-isopropylacrylamide) (PNIPAm) hydrogel. Differential volume changes between swellable PNIPAm and nonswellable PLA induce programmable shape transformation of the PNIPAm/PLA composite sheets. PLA strips are very stiff with Young's modulus higher than that of PNIPAm by five orders of magnitude, such that the preferred folded configuration of PNIPAm/PLA composite sheets is for the folding axis to orient parallel to the rigid PLA strips, in good agreement with the results of finite element simulations. It is worth noting that our work differs from most existing self-shaping strategies exploiting bilayer mechanism for which folding axes were perpendicular to the embedded fibers. Various 3D configurations are achieved by programming the embedded PLA patterns. Examples of configurations attained include tubes, scrolls, helixes, and complex shapes such as the analog of curled leaves. We hope this work can provide mechanistic guidance for creating new self-morphing and stimuli-responsive machines by integrating both hard and soft materials with considerable difference in modulus.

2. Design of shape-morphing composite sheets with hard and soft materials

2.1. Finite element simulation

To instruct the design of composite sheets, we started with finite element modeling to investigate the shape transformation of the composite sheets that contain plastic fibers embedded in the soft hydrogel matrix, with the fibers located near the bottom surface of the composite sheet (Fig. 1). It is worth noting that the development of shape-morphing composite sheets usually adopts embedded fibers with the fiber size comparable to the characteristic size of the overall sheets [12,18,25,26,31]. Therefore, in this study, we use a set of representative dimensions (including fiber size, fiber spacing, thickness of the overall sheets, etc.) commonly used in constructing composite sheets, and focus on how the change of constituent materials (reflected by the variation in modulus) affects the folding behavior. The plastic fibers are taken to be a linearly-elastic material, while the material behavior of the hydrogel phase is modeled by the modified Flory–Huggins theory developed by Hong and Suo [40]. Accordingly, the modulus of the plastic fibers and the hydrogel matrix are characterized by the Young's modulus E and the initial shear modulus NkT of the hydrogel, respectively. Note that N is the nominal density of polymer chains defined as the number of polymer chains divided by the volume of dry polymer network, k is the Boltzmann constant, and T is the temperature in the Kelvin scale. We first study the shape transformation of a square hydrogel sheet with plastic strips oriented perpendicular to one side of the square (as illustrated in Fig. 1a, the white line on the top surface of the sheet is added to highlight the orientation of the fibers embedded in the hydrogel matrix). The geometry and dimensions of the simulation model are given in Fig. A.1(a). When the hydrogel matrix dehydrates and shrinks in volume, geometrical mismatch between deswelled hydrogel and non-swellable plastic fibers leads to the rolling up of the hybrid hydrogel sheets into a tubular structure. Our simulations suggest that the variation in the modulus ratio between plastic fibers and the hydrogel matrix significantly affects the orientation of the rolling axis of hybrid sheets, thereby giving rise to different preferred morphologies of hybrid sheets. In the numerical examples below, we set the Poisson's ratio of the fiber and the dimensionless parameter measuring entropy of mixing of the hydrogel to be 0.3 and 0.1 [40], respectively, and vary the modulus ratio between the plastic fibers and the hydrogel matrix. When the modulus ratio is comparatively small (e.g., $E/NkT = 1$ or 10), the shrinkage of the hydrogel results in the rolling up of the 2D hydrogel sheet into a tubular structure, and the folding axis is perpendicular to the plastic fibers, forcing the plastic fibers to bend (Fig. 1b and c). In stark contrast, when the modulus ratio E/NkT increases to 100 and beyond, i.e., the composite sheets are made from integrating hydrogel matrix and very hard fibers, the hybrid hydrogel sheets roll up along an axis parallel to the plastic fibers, without stretching or bending the hard fibers (Fig. 1d–f). To further understand the role of modulus ratio in the shape transformation, we also investigate square hydrogel sheets with strips making an angle of 45° with respect to the sides of the square sheets (Fig. 1g). The dimensions of the model are shown in Fig. A.1(b). The dehydration of hydrogel matrix drives the hybrid hydrogel sheets to fold into a taco-shaped structure. The folding axis is perpendicular to the comparatively compliant plastic strips for $E/NkT = 1$ (Fig. 1h) and 10 (Fig. 1i), while parallel to the rigid plastic fibers for $E/NkT = 100$ (Fig. 1j), 1000 (Fig. 1k), and 10000 (Fig. 1l). The trend is in good agreement with the cases shown in Fig. 1b–f. The physical mechanism underpinning the folding axis can be analyzed from a mechanical point of view. Shape transformation of hybrid sheets occurs to release elastic energy accumulated due to differential shrinkage of the hydrogel and plastic fibers, such that the final shape of the hybrid sheets should be minimal in terms of strain energy. When the modulus of plastic fibers exceeds that of hydrogel by orders of magnitude, for example, $E/NkT = 100$ and beyond. Any deformation of the stiff plastic fibers leads to considerable strain energy, such that folding of the hybrid sheet prefers a final configuration with minimized bending of plastic fibers. That is to say, folding takes place along the plastic strips, with the rolling axis parallel to the strip orientation, as shown in Fig. 1d–f and Fig. 1j–l.

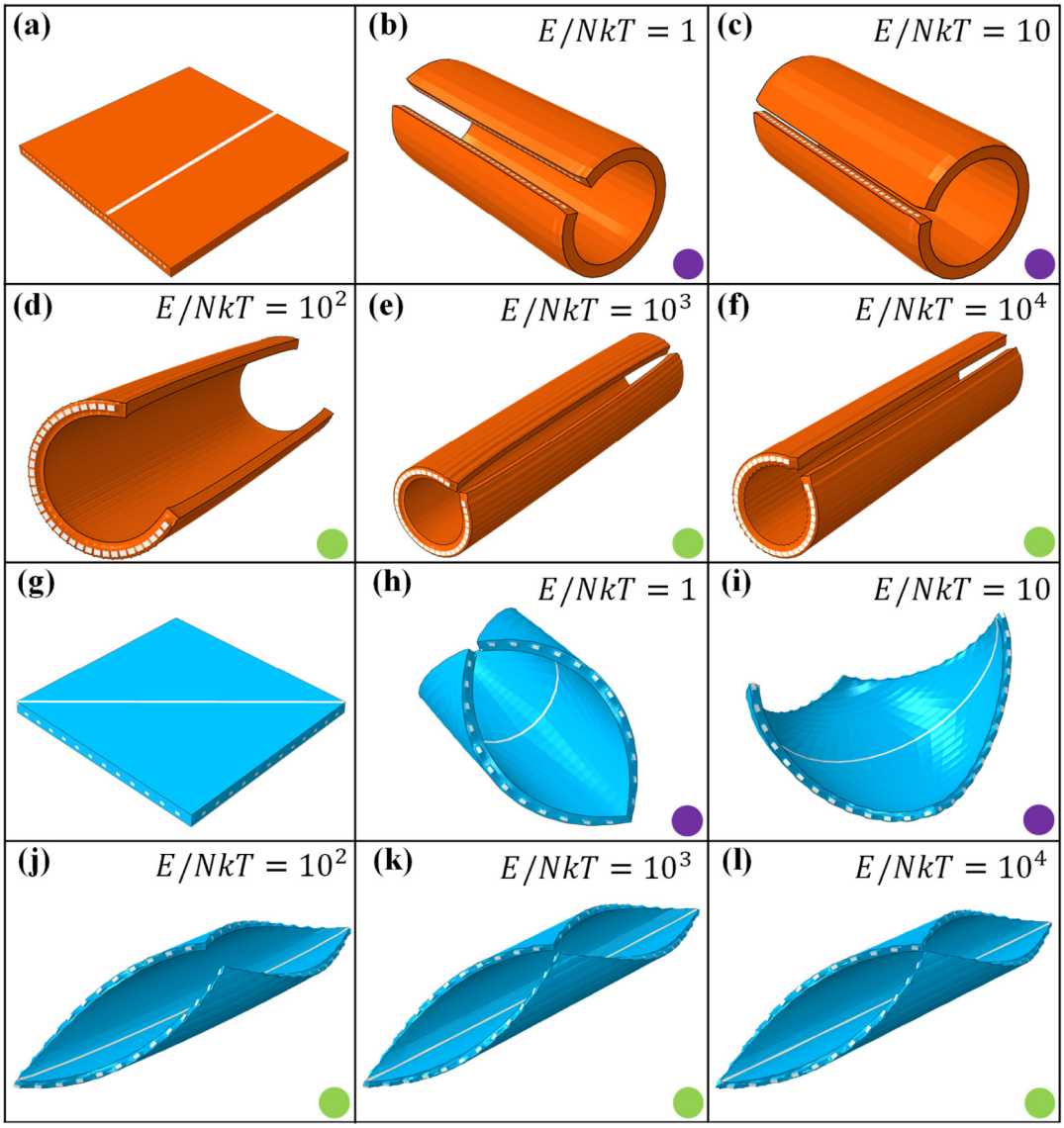

Fig. 1. Shape transformation of hybrid hydrogel sheets predicted by finite element modeling. The hybrid sheets consist of plastic fibers (white color) embedded in a hydrogel matrix. (a) Schematic of the initial configuration of a square hybrid sheet. The embedded fibers are oriented perpendicular to one side of the square. The white line is added to visualize the orientation of the plastic fibers. (b–f) Modeling of the shape transformation of the hybrid sheets with modulus ratio E/NkT ranging from 1 to 10^4. (g) Schematic of a square hybrid sheet with embedded fibers oriented parallel to the diagonal of the square sheet. The white line marks the orientation of the plastic fibers. (h–l) FEM results of the shape transformation of the hybrid sheets with modulus ratio E/NkT ranging from 1 to 10^4. It is revealed that the orientation of the folding axis is dictated by the modulus ratio E/NkT: the folding axis is parallel to the plastic fibers for composite sheets with rigid fibers (d–f, j–l), while the folding axis is perpendicular to the plastic fibers for composite sheets with comparatively soft fibers (b–c, h–i). Note that the purple dots and green dots are used to highlight the orientation of the folding axis: purple dots indicate the rolled structure has folding axis perpendicular to fibers, while green dots are indicative of folding axis parallel to fibers. (For interpretation of the references to color in this figure legend, the reader is referred to the web version of this article.)

2.2. Fabrication of PNIPAm/PLA composites

Most reported shape-morphing composite structures containing strips embedded in hydrogel matrix exhibit folding axis perpendicular to the embedded strips [12,18,25,31]. Instructed by the findings from simulations, we have fabricated hybrid sheets by integrating extremely hard fibers and soft hydrogels. One salient feature of our composite sheets is the folding axis oriented parallel to the embedded fibers, in contrast to most reported hybrid hydrogel sheets featuring folding axis normal to the embedded fibers. It is conceivable that such hybrid sheets can be constructed by various approaches and materials. This paper adopts PLA as the embedded fibers and PNIPAm hydrogel as the matrix. PLA (MakerBot, USA) is a stiff thermoplastic polyester and does not swell in water. We utilized a 3D printer MakerBot Replicator + (MakerBot, USA) to fabricate the PLA patterns for its simplicity and versatility. PLA samples were produced at room temperature while the nozzle temperature was controlled at 230 °C. The printing speed was set to be 150 mm/s and the thickness of each PLA filament extruded through the nozzle was fixed at 100 μm. A representative printed sample, i.e., a rectangular construct with PLA arranged in parallel strips, is sketched in Fig. 2a. The sample contains two parts: PLA strips with programmed distributions and orientations, and a frame supporting the PLA strips. Each PLA strip consists of 5–6 layers of filaments and exhibits a rectangular-shaped cross-section with a width of W = 600 μm and a thickness about 500 μm. The strip distribution and orientation are characterized by the distance

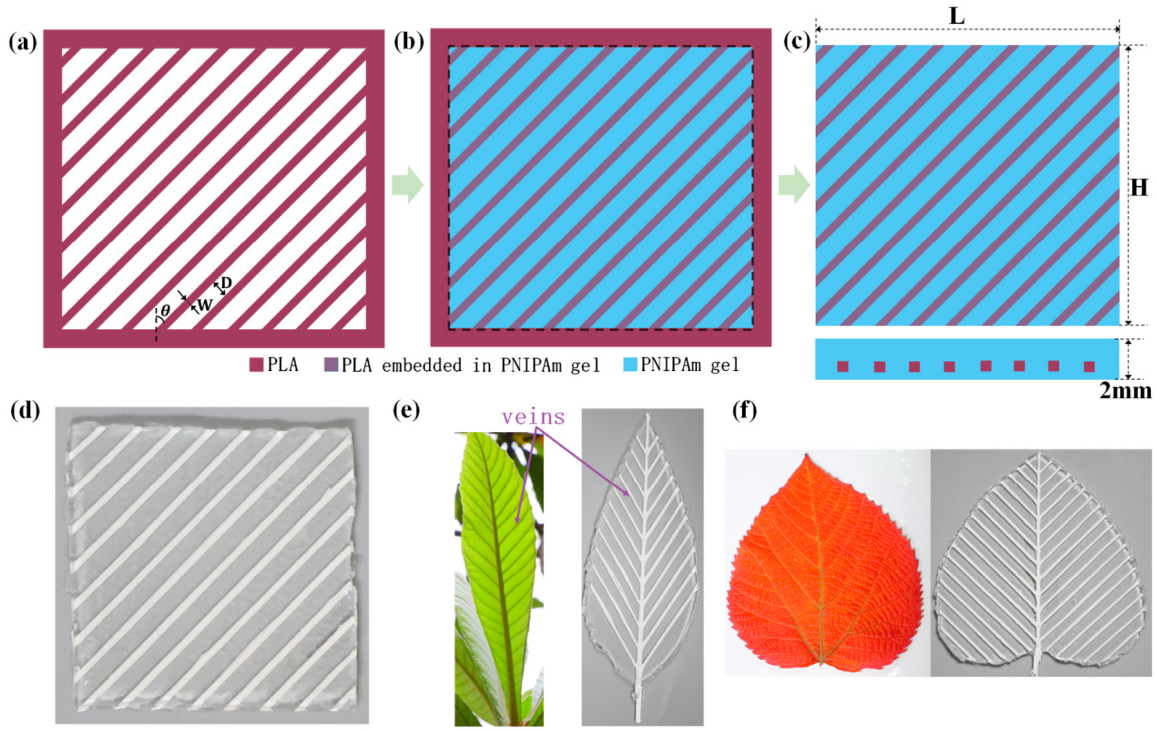

Fig. 2. 3D-printing-assisted fabrication of PNIPAm/PLA composite sheets. (a) Schematic of the 3D-printed PLA pattern comprised of PLA strips distributed in a parallel manner and a frame supporting the strips. The distribution and orientation of strips are specified by three parameters: the width of the PLA strips (W), the distance between adjacent strips (D), and the fiber orientation angle (θ). (b) PNIPAm pre-gel solution is infused into the mold slowly, with all PLA strips immersed in the solution. (c) After polymerization, we cut off the supporting frame along the black dashed line, resulting in the final PNIPAm/PLA composite sheet with PLA strips embedded in PNIPAm matrix. The in-plane dimensions of the sheet are given by L × H. (d) Photograph of the as-fabricated 2D PNIPAm/PLA sheets. The white strips are PLA and the transparent regions are PNIPAm gels. (e–f) Nature-inspired designs of composite sheets that resemble (e) the lanceolate leaf and (f) the cordate leaf. The PLA patterns represent the vein structure. The thickness of all samples fabricated in this work is 2 mm unless stated otherwise.

D between neighboring strips and the strip orientation angle θ (Fig. 2a), respectively. Because of the flexibility endowed by 3D printing, these design parameters can be facilely changed to examine the effect of PLA patterns on the shape morphing of PNIPAm/PLA sheets.

To construct the PNIPAm/PLA composite sheets, we prepared a pre-gel solution by dissolving powders of N-isopropylacrylamide (3A chemicals Co. Ltd, A11254) in deionized water. We added ammonium persulfate (APS) (Sinopharm Chemical Reagent Co., Ltd, 10002616) as the thermal initiator, N,N-methylenebisacrylamide (MBAA) (Sinopharm Chemical Reagent Co., Ltd, 80120061) as the crosslinker, and N,N,N′,N′-tetramethylethylenediamine (TEMED) (Aladin, T140800) as the initiation accelerator. The detailed recipe of the hydrogel is given in Table B.1 of the appendix. The 500 μm-thick PLA structure printed in the previous step (Fig. 2a) was placed in a 2 mm-thick acrylic mold, covered with a 2 mm-thick acrylic plate. The PNIPAm pre-gel solution was slowly infused into the acrylic mold. Thereafter, the gel was left at room temperature for 12 h to polymerize, resulting in a PNIPAm/PLA hybrid structure as illustrated in Fig. 2b. After the polymerization step, the as-fabricated PNIPAm/PLA composite sheets were rinsed with sterile water for several times to remove the unreacted monomer and other impurities. Lastly, we cut off the outer PLA supporting frame along the reference line (i.e., dash lines in Fig. 2b) and obtained the final PNIPAm/PLA composite sheets (Fig. 2c). The photograph of a prototypical example of as-fabricated PNIPAm/PLA sheets is shown in Fig. 2d, with white strips being PLA and the transparent matrix PNIPAm. As illustrated in Fig. 2c, PLA strips are embedded in the PNIPAm gel and located near the bottom surface of the sheet, such that the composites can be considered as a "bilayer". The top layer contains only PNIPAm gel so that it is referred to as the PLA-free layer hereafter, the bottom layer has PLA fibers uniformly distributed in PNIPAm gels and is thus referred to as the PLA-rich layer. As will be discussed later, such "bilayer" structures give rise to strong out-of-plane mismatch in mechanical properties and responsiveness to stimuli, and thus the composite could be induced to transform into 3D morphologies by temperature change. Furthermore, to imitate the self-shaping phenomena in natural systems, we also created lanceolate (Fig. 2e) and cordate (Fig. 2f) PNIPAm/PLA hybrid sheets following the same procedure presented above, with the 3D-printed PLA patterns mimicking the leaf veins.

3. Shape morphing of PNIPAm/PLA composite sheets with FEM-predicted folding axis

3.1. Folding of planar PNIPAm/PLA composite sheets

Guided by the results of FEM simulations (Fig. 1a–f), we first studied the response of a square-shaped PNIPAm/PLA composite sheet with PLA strips oriented perpendicular to one side of the square (Figs. 3a, e and 4a). The dimensions of the sheet are 45 mm (L) × 45 mm (H) × 2 mm (T). To induce the shape transformation of PNIPAm/PLA composites, the as-fabricated hybrid sheets were submerged in water at room temperature, followed by heating the water to 45 °C, above the temperature of dehydration of PNIPAm but below the glass transition temperature of PLA. The as-fabricated hybrid composite was initially a flat sheet and remained so when immersed in water at room temperature (Fig. 3e). However, when the water temperature reached 40 °C, beyond the Lower Critical Solution Temperature (LCST) of PNIPAm, the composite began to roll up and eventually folded into a tubular structure, as shown in Figs. 3f and 4a. Such shape transformation phenomena can be understood in two-folds: (1)

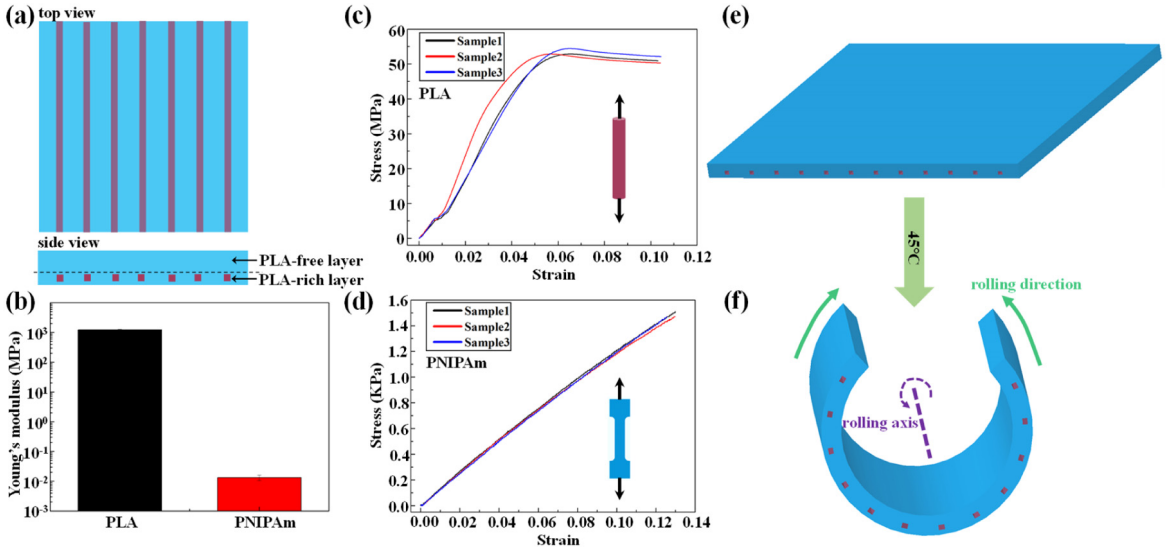

Fig. 3. Mechanism for PNIPAm/PLA composite sheet folding. (a) The schematic of a square-shaped composite sheet. The side view indicates that the sheet is comprised of a PLA-free layer as well as a PLA-rich layer. (b) Young's moduli, i.e., the measure of modulus, of the PNIPAm and PLA. It is shown that the modulus of PLA strip exceeds that of PNIPAm matrix by five orders of magnitude. (c–d) The stress–strain curves of PLA and PNIPAm, from which Young's moduli are extracted. (e–f) Schematics of the shape-morphing process. When exposed to water of 45 °C, the composite sheet folds towards the PLA-free side. As predicted by the FEM simulations, the rolling axis is well specified by the orientation of stiff PLA strips: the axis is parallel to the PLA strips.

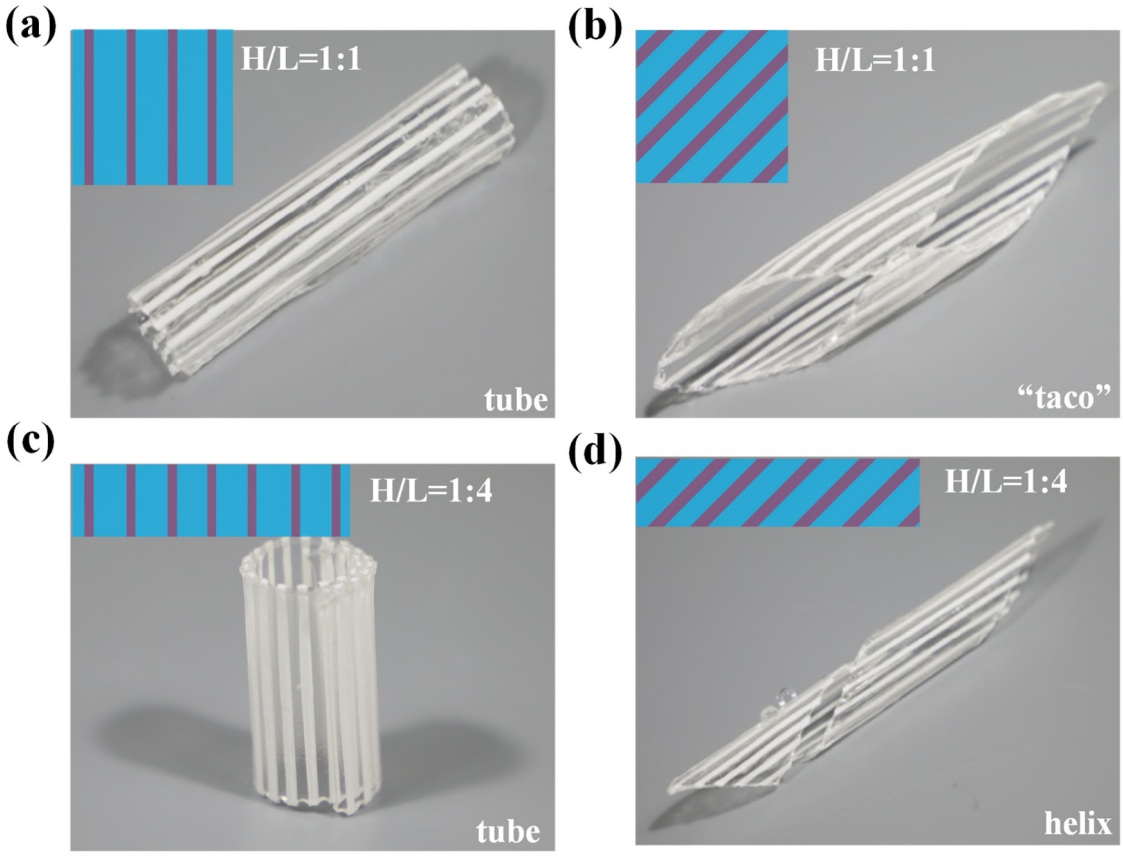

Fig. 4. Photographs of 3D configurations adopted by PNIPAm/PLA composite sheets upon exposure to elevated temperature. The white strips correspond to PLA, while the transparent regions are PNIPAm gel. The colored insets show schematics of corresponding initial 2D configurations before shape transformation. (a) A tubular structure formed in deionized water of 45 °C by a square PNIPAm/PLA composite sheet with PLA patterned in parallel strips. The strips are orientated with $\theta = 0°$. (b) A taco-like structure generated by a square sheet with PLA strips making an orientation angle of $\theta = 45°$. (c) A tubular structure formed by a rectangular PNIPAm/PLA sheet characterized by an aspect ratio of H/L = 1:4 and orientation angle of $\theta = 0°$. (d) A helical structure acquired by a rectangular PNIPAm/PLA sheet with H/L = 1:4 and $\theta = 45°$. The thickness of the composite sheet is 2 mm. All strips are uniformly distributed with distance D between adjacent strips fixed by D/W = 5:1.

The folding direction. Upon an increase in temperature, PNIPAm gel shrunk significantly by expelling a large amount of water, whereas PLA does not change its volume. In consequence, the PLA-free layer shrunk much more than the PLA-rich layer, driving the "bilayer" hybrid sheet to roll up towards the PLA-free side (Fig. 3f). (2) The folding axis. The final morphology of the PNIPAm/PLA sheet is not only characterized by the folding direction, but also by the folding axis. For composite sheets with only soft constituent materials, considerable effects need to be made to precisely control the folding axis by carefully tailoring the mechanical properties of the constituent materials [12,15]. For example, the composite sheets comprised of laponite-crosslinked PNIPAm matrix and BIS-crosslinked PNIPAm strips may roll up along an axis either parallel or perpendicular to the strips [12], depending on the crosslinking density of the constituent materials. In this work, guided by the results of FEM simulations, the folding axis is well predicted: the PNIPAm/PLA hybrid sheets always fold along the stiff PLA strips since the modulus of PLA strips is sufficiently large compared to the hydrogel matrix.

Instructed by the FEM results shown in Fig. 1j–l, we also construct a square-shaped hybrid sheet with PLA strips making an orientation angle of $\theta = 45°$. The composite sheet also folds along the PLA strips (Fig. 4b), generating a taco-shaped structure, which is well in line with the FEM results shown in Fig. 1j–l. We also explored the effect of the aspect ratio of composite sheets. Tubular and helical shapes were achieved by changing the aspect ratio H/L to 1:4 (Fig. 4c and d). The results explicate that the folding axis is intrinsic to the arrangement of hard PLA strips as predicted by the FEM modeling and do not depend on the aspect ratio of the overall hybrid: The folding axis is always parallel to the PLA strips.

3.2. Analog of curled leaf

Although the self-shaping of hybrid sheets discussed above is interesting on its own in terms of the fundamental mechanics underpinning the folding axis, the PLA pattern used was still simple and idealized, especially when considering that distribution and orientation of cellulose fibers in plant tissues are much more complicated. By taking advantage of 3D printing technique, we can incorporate more complex PLA patterns into PNIPAm gels to engineer biomimicking shape transitions. As an example, we designed a curled leaf analog by using PANIPAm/PLA hybrid sheets, with the purpose of demonstrating the applicability of our approach to engender complex shape transformation and unraveling how stiff veins dictate the curling of leaves induced by dehydration.

As the most visible traits of leaves, veins are vascular structures that transport water and carbohydrate and mechanically maintain the shape of leaves [41–43]. Vein patterns are tailored by nature to specific functions of leaves, such that these patterns vary significantly between disparate species. In terms of the arrangement of primary veins (i.e., the vein entering the leaf from the petiole), vein patterns can be classified as pinnate, palmate, and parallel [42]. Leaves with pinnate venation feature a single primary vein running through the length of the leaf, with secondary veins branching from the primaries and ending at the leaf margin (Figs. 2e–f and 5b). Herein, to demonstrate the feasibility of our approach in generating complex 3D morphologies, we fabricated PNIPAm/PLA composite sheets to mimic the curling of pinnate-veined leaves due to dehydration. PLA strips representing the pinnate vein patterns were constructed by 3D printing, with elaborately designed overall leaf shape and orientation of secondary veins. Two types of leaf shapes, including a lanceolate leaf (Fig. 5a) and a cordate leaf (Fig. 6a), and four orientation angles including 15°, 30°, 45°, and 60° were adopted. Thereafter, as noted above, we made our mimic of leaves by incorporating fabricated PLA patterns into PNIPAm hydrogels representing the lamina and epidermis of plant leaves. The as-made composite sheets reminiscent of lanceolate leaves are shown in Fig. 5b, which is characterized by a long and narrow shape. Once immersed in hot water between 40 °C and 45 °C, the sheets began to dehydrate and fold. As expected, the folding of composite sheets occurs along the parallel rigid PLA strips. Here, the PLA pattern is symmetric with respect to the primary vein, with all secondary veins arranged in parallel strips at an orientation angle θ (Fig. 5b), thus the folding guided by the parallel secondary veins leads to an overall bending of the leaf along an axis perpendicular to the primary vein. The degree of curling depends on the angle θ: a lanceolate sample featuring larger orientation angle θ of secondary veins bends more than its smaller-angle counterpart, as evident by Fig. 5c–f. Notably, the folded samples resemble the curled shape of many dehydrated leaves in nature, which indicates that the curling process of these leaves might be governed by the local folding along the hard veins.

To further visualize the directional folding dictated by the stiff secondary veins, we studied the shape transformation of heart-shaped sheets that resemble the cordate leaves (Fig. 6a and b). In stark contrast to the long and narrow lanceolate leaf, the cordate leaf has a broad blade, such that the two half blades are sufficiently large to roll up by itself. When the orientation angle θ of secondary veins is small (e.g., $\theta = 15°$, Fig. 6c), i.e., the primary and secondary veins are almost along the same direction, the two halves of leaf blade rolled up along the stiff secondary veins separately, with the primary vein almost undeformed. As the angle increased to 30°, the secondary veins are apparently inclined to the primary vein, so that folding along the secondary veins led to simultaneous curling up of half blades and bending of the primary vein (Fig. 6d). When θ further increased to 45°, the degree of global bending increased, with the local curling becoming less visible (Fig. 6e). For large orientation angle of 60°, the local rolling up of the two half blades vanished. Instead, deformation of the leaf was dominated by the global bending of the primary vein, similar to the shape transition of a lanceolate leaf (Fig. 6f). In closing, via constructing the analog of curled leaves by integrating hard PLA fibers and soft hydrogel matrix, we speculate that the curling process of many leaves in nature is governed by the local folding of soft blades along the rigid veins.

4. Conclusion

We have conducted finite element modeling to simulate the shape transformation of hybrid sheets that consist of polymer strips embedded in the hydrogel matrix, which is a widely employed approach to achieve self-folding structures. It is revealed that the orientation of the folding axis is parallel to the hard fibers when the fiber modulus is significantly larger than that of the hydrogel matrix. Note that most shape-morphing composite structures containing strips embedded in hydrogel matrix exhibit folding axis perpendicular to the embedded strips [12,18,25,31]. Instructed by the findings from mechanistic simulations, we have fabricated hybrid hydrogel sheets featuring folding axis parallel to the embedded fibers by integrating 3D-printed hard PLA fibers and soft PNIPAm hydrogel. Given the fact that modulus of PLA exceeds that of PNIPAm by five orders of magnitude, folding of composite sheets favor a final morphology with minimal deformation of PLA fibers, such that the sheets roll up along the PLA strips (namely, with the rolling axis parallel to the strip orientation), which is well in line with results of finite element modeling. Various 3D shapes, such as scrolls, helices, and tubes, can be achieved by the geometric design of embedded

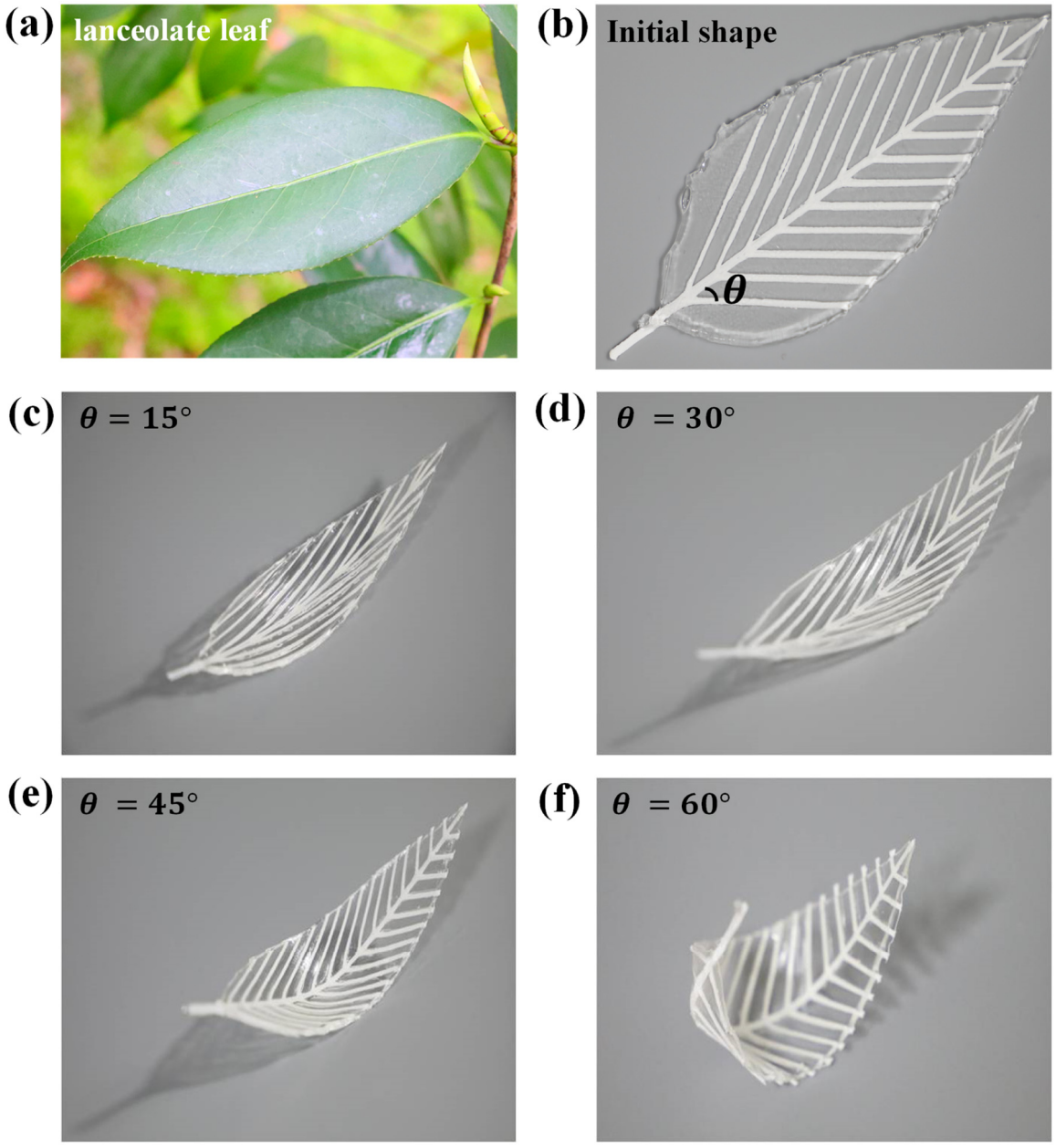

Fig. 5. PNIPAm/PLA composite sheets that imitate the dehydration behavior of a lanceolate leaf. (a) A photograph of a lanceolate leaf. (b) The design of PNIPAm/PLA composite sheet that mimics the lanceolate leaf with pinnate venation, which features a primary vein running through the length of the leaf, with secondary veins branching from the primary vein and ending at the leaf margin. The vein patterns are quantified by the strip orientation angle $\theta = 15°$ (c), 30° (d), 45° (e) and 60° (f), respectively. The PNIPAm/PLA hybrid was initially a flat sheet. (c–f) When exposed to hot water of 45 °C, the composite sheet dehydrated and folded along the secondary veins, causing various degrees of bending of the entire sheet. The composite sheet with higher value of θ bends more than its counterpart with smaller θ. The leaf is 2 mm in thickness.

PLA patterns via 3D-printing technique. The versatility of our approach is demonstrated by engineering the folding of flat sheets into more complex 3D configurations. For example, we designed structures reminiscent of pinnate-veined leaves. These structures folded when exposed to temperature change, which mimics the dehydration-induced curling of leaves. Local rolling and global bending of the leaf analog were induced by the secondary-vein-dictated directionality for folding. The research findings offer mechanistic understandings of the curling process of leaves in nature. We hope this work can provide mechanistic guidance for designing shape-morphing soft machines that are made by harnessing both hard and soft constituent materials.

Declaration of competing interest

The authors declare that they have no known competing financial interests or personal relationships that could have appeared to influence the work reported in this paper.

Acknowledgments

This work is supported by the National Natural Science Foundation of China (No. 11802269, No. 11525210, and No. 11621062). The authors acknowledge the Fundamental Research Funds for the Central Universities, China. Zheng Jia also acknowledges the

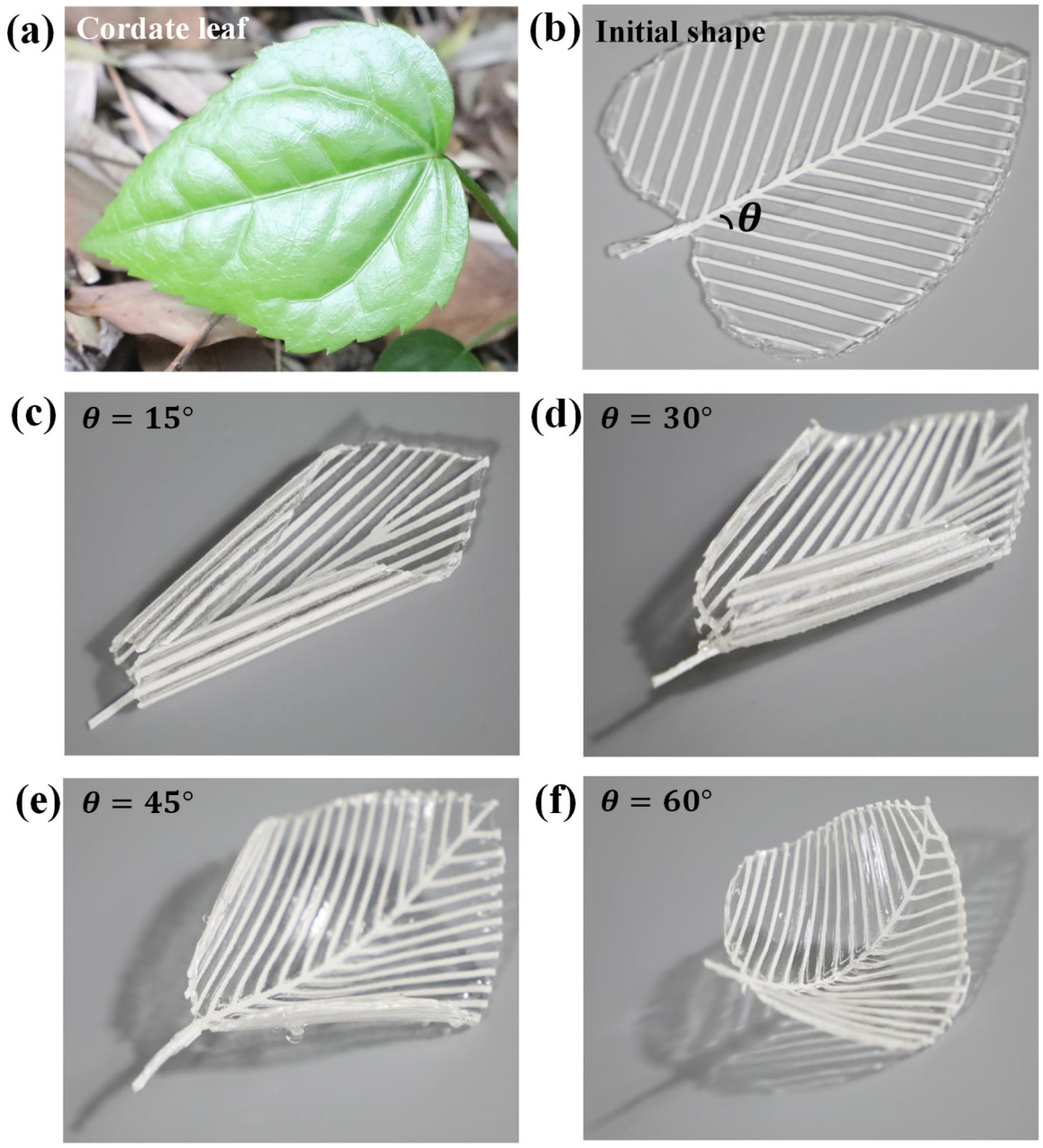

Fig. 6. PNIPAm/PLA sheets that mimic the curling of a cordate leaf. (a) The natural inspiration for the design comes from the cordate leaf, which is large and broad. (b) The photograph of a PNIPAm/PLA composite sheet that mimics the pinnate-veined cordate leaf. (c) For small orientation angle of $\theta = 15°$, shape transformation of the leaf was dominated by the local curling of the two half blades, leaving the primary vein almost undeformed. (d) As θ was increased to 30°, local curling of half blades and global bending of the primary vein occurred simultaneously. (e) When θ attained 45°, the degree of global bending increased, while the local curling became less visible. (f) For $\theta = 60°$, global bending prevailed over local curling. The deformed 3D morphology was similar to that of a lanceolate leaf.

financial support from the One-Hundred Talents Program of Zhejiang University, China.

Appendix A. Dimensions and geometry of the finite element model

To understand the shape transformation of the composite sheets that contain plastic fibers embedded in the soft hydrogel matrix , we simulated two representative structures: (i) square hydrogel sheets with plastic strips oriented perpendicular to one side of the square, and (ii) square hydrogel sheets with strips making an angle of 45° with respect to the sides of the square sheets. Dimensions of the two representative models are given in Fig. A.1.

Appendix B. The recipe of the PNIPAm hydrogels

We add 133.67 μL of APS (0.2M) as the thermo initiator, 40 μL of MBAA (0.1M) as the crosslinker and 1 μL of TEMED (pure) as the initiation accelerator into 10 mL of NIPAm (2M) monomer solution. Detailed recipe is given in Table B.1.

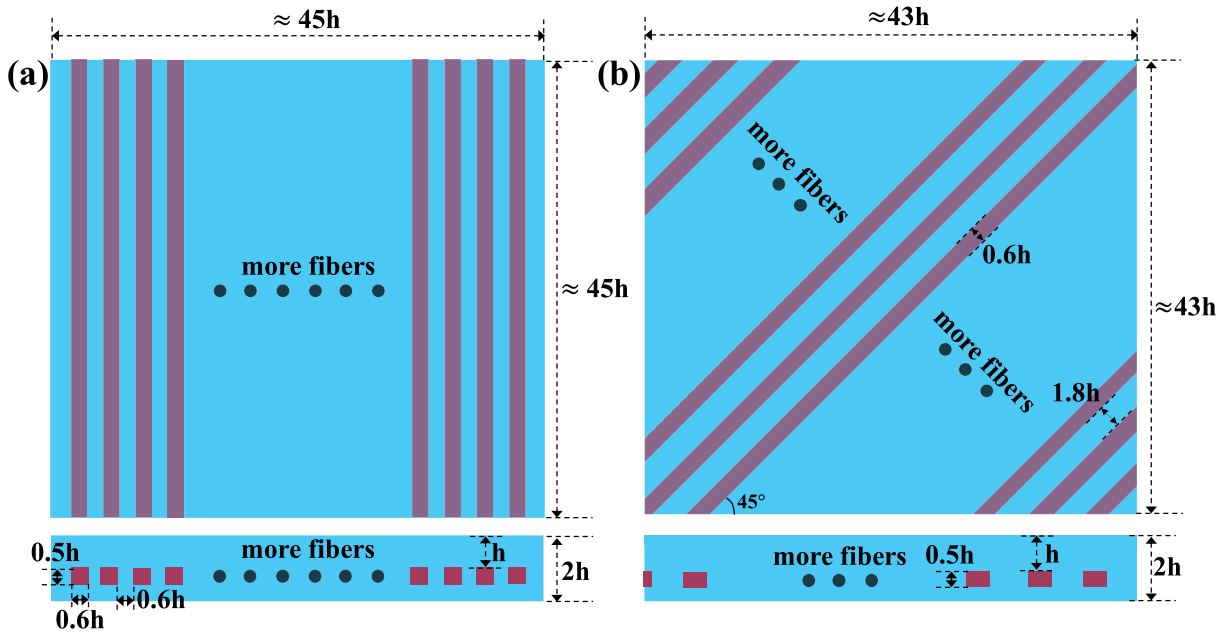

Fig. A.1. The geometry and dimensions of the PNIPAm/PLA composite sheets simulated in finite element modeling. (a) Case 1: the PLA fibers are perpendicular to one side of the square sheet. (b) Case 2: the fibers make an inclination angle of 45° to both sides of the square sheet.

Table B.1
Recipe for the synthesis of PNIPAm hydrogel. N-isopropylacrylamide (NIPAm) was from 3A chemicals (3A chemicals Co. Ltd, A11254), N,N,N′,N′-tetramethylethylenediamine (TEMED) was from Aladin (Aladin, T140800), Ammonium persulfate (APS) and N,N-methylenebisacrylamide (MBAA) were from Sinopharm Chemical Reagent limited corporation (Sino harm Chemical Reagent Co., Ltd, 10002616,80120061). A pre-gel solution of poly-N-isopropylacrylamide (PNIPAm) was prepared by adding APS as the thermal initiator, MBAA as the crosslinker and TEMED as the initiation accelerator to the NIPAm solution.

NIPAm (2M) (mL)	APS (0.2M) (μL)	MBAA (0.1M) (μL)	TEMED (μL)
10	133.67	40	1

References

[1] Y. Forterre, J.M. Skotheim, J. Dumais, L. Mahadevan, Nature 433 (2005) 421–425.
[2] H. Liang, L. Mahadevan, Proc. Natl. Acad. Sci. USA 108 (2011) 5516–5521.
[3] M.J. Harrington, K. Razghandi, F. Ditsch, L. Guiducci, M. Rueggeberg, J.W.C. Dunlop, P. Fratzl, C. Neinhuis, I. Burgert, Nature Commun. 2 (2011).
[4] R. Elbaum, L. Zaltzman, I. Burgert, P. Fratzl, Science 316 (2007) 884–886.
[5] S. Armon, E. Efrati, R. Kupferman, E. Sharon, Science 333 (2011) 1726–1730.
[6] S. Xu, Z. Yan, K.-I. Jang, W. Huang, H. Fu, J. Kim, Z. Wei, M. Flavin, J. McCracken, R. Wang, A. Badea, Y. Liu, D. Xiao, G. Zhou, J. Lee, H.U. Chung, H. Cheng, W. Ren, A. Banks, X. Li, U. Paik, R.G. Nuzzo, Y. Huang, Y. Zhang, J.A. Rogers, Science 347 (2015) 154–159.
[7] E. Hawkes, B. An, N.M. Benbernou, H. Tanaka, S. Kim, E.D. Demaine, D. Rus, R.J. Wood, Proc. Natl. Acad. Sci. USA 107 (2010) 12441–12445.
[8] C. Ahn, X. Liang, S. Cai, Adv. Mater. Technol. 4 (2019).
[9] R. Fernandes, D.H. Gracias, Adv. Drug Deliv. Rev. 64 (2012) 1579–1589.
[10] T.G. Leong, C.L. Randall, B.R. Benson, N. Bassik, G.M. Stern, D.H. Gracias, Proc. Natl. Acad. Sci. USA 106 (2009) 703–708.
[11] Z.B. Hu, X.M. Zhang, Y. Li, Science 269 (1995) 525–527.
[12] Z. Wei, Z. Jia, J. Athas, C. Wang, S.R. Raghavan, T. Li, Z. Nie, Soft Matter 10 (2014) 8157–8162.
[13] J. Li, Z. Suo, J.J. Vlassak, Soft Matter 10 (2014) 2582–2590.
[14] H. Therien-Aubin, Z.L. Wu, Z. Nie, E. Kumacheva, J. Am. Chem. Soc. 135 (2013) 4834–4839.
[15] J.C. Athas, C.P. Nguyen, S. Kummar, S.R. Raghavan, Soft Matter 14 (2018) 2735–2743.
[16] P. Techawanitchai, M. Ebara, N. Idota, T.-A. Asoh, A. Kikuchi, T. Aoyagi, Soft Matter 8 (2012) 2844–2851.
[17] H. Guo, J. Cheng, J. Wang, P. Huang, Y. Liu, Z. Jia, X. Chen, K. Sui, T. Li, Z. Nie, J. Mater. Chem. B 5 (2017) 2883–2887.
[18] J.C. Athas, C.P. Nguyen, B.C. Zarkett, A. Gargava, Z. Nie, S.R. Raghavan, ACS Appl. Mater. Interfaces 8 (2016) 19066–19074.
[19] Z. Chen, D. Zhao, B. Liu, G. Nian, X. Li, J. Yin, S. Qu, W. Yang, Adv. Funct. Mater. 29 (2019) 1900971.
[20] J. Tang, Z. Tong, Y. Xia, M. Liu, Z. Lv, Y. Gao, T. Lu, S. Xie, Y. Pei, D. Fang, T.J. Wang, J. Mater. Chem. B 6 (2018) 2713–2722.
[21] Y. Klein, E. Efrati, E. Sharon, Science 315 (2007) 1116–1120.
[22] J. Kim, J.A. Hanna, M. Byun, C.D. Santangelo, R.C. Hayward, Science 335 (2012) 1201–1205.
[23] H. Therien-Aubin, M. Moshe, E. Sharon, E. Kumacheva, Soft Matter 11 (2015) 4600–4605.
[24] S.Y. Zheng, Y. Shen, F. Zhu, J. Yin, J. Qian, J. Fu, Z.L. Wu, Q. Zheng, Adv. Funct. Mater. 28 (2018).
[25] Z.L. Wu, M. Moshe, J. Greener, H. Therien-Aubin, Z. Nie, E. Sharon, E. Kumacheva, Nature Commun. 4 (2013).
[26] Z.J. Wang, C.N. Zhu, W. Hong, Z.L. Wu, Q. Zheng, J. Mater. Chem. B 4 (2016) 7075–7079.
[27] H. Deng, Y. Dong, J.-W. Su, C. Zhang, Y. Xie, C. Zhang, M.R. Maschmann, Y. Lin, J. Lin, Acs Appl. Mater. Interfaces 9 (2017) 30900–30908.
[28] S. Janbaz, R. Hedayati, A.A. Zadpoor, Mater. Horiz. 3 (2016) 536–547.
[29] M. Li, D. Joung, D.K. Hwang, Langmuir 34 (2018) 6856–6860.
[30] Y. Liu, B. Shaw, M.D. Dickey, J. Genzer, Sci. Adv. 3 (2017).
[31] J. Tang, Q. Yin, Y. Qiao, T. Wang, Acs Appl. Mater. & Interfaces 11 (2019) 21194–21200.
[32] A.R. Studart, R.M. Erb, Soft Matter 10 (2014) 1284–1294.
[33] S.-J. Jeon, R.C. Hayward, Adv. Mater. 29 (2017).
[34] J. Guo, T. Shroff, C. Yoon, J. Liu, J.C. Breger, D.H. Gracias, T.D. Nguyen, Extreme Mech. Lett. 16 (2017) 6–12.
[35] J.C. Breger, C. Yoon, R. Xiao, H.R. Kwag, M.O. Wang, J.P. Fisher, T.D. Nguyen, D.H. Gracias, Acs Appl. Mater. Interfaces 7 (2015) 3398–3405.
[36] A.S. Gladman, E.A. Matsumoto, R.G. Nuzzo, L. Mahadevan, J.A. Lewis, Nature Mater. 15 (2016) 413–418.
[37] Q. Ge, H.J. Qi, M.L. Dunn, Appl. Phys. Lett. 103 (2013).
[38] Y. Mao, Z. Ding, C. Yuan, S. Ai, M. Isakov, J. Wu, T. Wang, M.L. Dunn, H.J. Qi, Sci. Rep. 6 (2016).
[39] L. Huang, R. Jiang, J. Wu, J. Song, H. Bai, B. Li, Q. Zhao, T. Xie, Adv. Mater. 29 (2017).
[40] W. Hong, Z. Liu, Z. Suo, Int. J. Solids Struct. 46 (2009) 3282–3289.
[41] A.G. Rolland-Lagan, M. Amin, M. Pakulska, Plant J. : Cell Mol. Biol. 57 (2009) 195–205.
[42] R.L. Walls, Am. J. Bot. 98 (2011) 244–253.
[43] Z. Sun, T. Cui, Y. Zhu, W. Zhang, S. Shi, S. Tang, Z. Du, C. Liu, R. Cui, H. Chen, X. Guo, Sci. Rep. 8 (2018).